Preinspiratory calcium rise in putative pre-Bötzinger complex astrocytes

Yasumasa Okada[1,2], Takuya Sasaki[3], Yoshitaka Oku[4], Naoya Takahashi[3], Megumi Seki[3], Sakiko Ujita[3], Kenji F. Tanaka[5], Norio Matsuki[3] and Yuji Ikegaya[3]

[1]*Division of Internal Medicine and Laboratory of Electrophysiology, Murayama Medical Center, Musashimurayama, Tokyo 208-0011, Japan*
[2]*Division of Pulmonary Medicine, Department of Internal Medicine, School of Medicine, Keio University, Tokyo 160-8582, Japan*
[3]*Laboratory of Chemical Pharmacology, Graduate School of Pharmaceutical Sciences, The University of Tokyo, Tokyo 113-0033, Japan*
[4]*Department of Physiology, Hyogo College of Medicine, Hyogo 663-8501, Japan*
[5]*Department of Neuropsychiatry, School of Medicine, Keio University, Tokyo 160-8582, Japan*

Key points

- Autonomic respiratory rhythm is essential to maintain lives and is generated in the lower brainstem. The ventrolateral medullary region, called the pre-Bötzinger complex (preBötC), is the kernel for respiratory rhythm generation. Despite previous extensive studies focusing on neurons, the mechanism of how respiratory rhythm is generated has not been fully understood.
- Here we show that non-neuronal glial cells (a subset of putative astrocytes) in the preBötC are periodically activated preceding inspiratory neuronal activity, periodic activity of putative astrocytes persists during blockade of neuronal activity, and stimulation of astrocytes in the preBötC induces inspiratory neuronal firings.
- These findings together with the previous report that blockade of astrocytic metabolism abolishes inspiratory neural output suggest that astrocytes are functionally involved in respiratory rhythm generation.
- These results will help us better understand how respiratory rhythm is generated and how respiratory output is disturbed in various pathological conditions.

Abstract The neural inspiratory activity originates from a ventrolateral medullary region called the pre-Bötzinger complex (preBötC), yet the mechanism underlying respiratory rhythmogenesis is not completely understood. Recently, the role of not only neurons but astrocytes in the central respiratory control has attracted considerable attention. Here we report our discovery that an intracellular calcium rise in a subset of putative astrocytes precedes inspiratory neuronal firing in rhythmically active slices. Functional calcium imaging from hundreds of preBötC cells revealed that a subset of putative astrocytes exhibited rhythmic calcium elevations preceding inspiratory neuronal activity with a time lag of approximately 2 s. These preinspiratory putative astrocytes maintained their rhythmic activities even during the blockade of neuronal activity with tetrodotoxin, whereas the rhythm frequency was lowered and the intercellular phases of these rhythms were decoupled. In addition, optogenetic stimulation of preBötC putative astrocytes induced firing of inspiratory neurons. These findings raise the possibility that astrocytes in the preBötC are actively involved in respiratory rhythm generation in rhythmically active slices.

(Resubmitted 29 February 2012; accepted after revision 6 July 2012; first published online 9 July 2012)
Corresponding author Y. Okada: Division of Internal Medicine and Laboratory of Electrophysiology, Murayama Medical Center, 2-37-1 Gakuen, Musashimurayama, Tokyo 208-0011, Japan. Email: yasumasaokada@1979.jukuin.keio.ac.jp

DOI: 10.1113/jphysiol.2012.231464

Abbreviations aCSF, artificial cerebrospinal fluid; ChR2, channelrhodopsin-2; CV, coefficient of variation; F, fluorescence intensity; I_{CAN}, non-specific cationic current; I_{NaP}, persistent sodium current; MLC, megalencephalic leukoencephalopathy with subcortical cysts; OGB1, Oregon Green 488 BAPTA-1 AM; PC, principal component; preBötC, pre-Bötzinger complex; ROI, region of interest; tTA, tetracycline transactivator; YFP, yellow fluorescent protein.

Introduction

Medullary slice preparations made of neonatal rodents that contain the pre-Bötzinger complex (preBötC), termed rhythmically active slices (Del Negro *et al.* 2011), exhibit spontaneous inspiratory-related rhythmic activity *in vitro* (Smith *et al.* 1991) and have been widely used to investigate the mechanism of respiratory rhythm generation. Although various hypotheses have been proposed to explain the mechanism of rhythmogenesis in this region, many of which are based on single neuron kinetics and neuronal network dynamics (Koshiya & Smith, 1999; Feldman & Del Negro, 2006; Pace *et al.* 2007; Koizumi & Smith, 2008; Rubin *et al.* 2009; Morgado-Valle *et al.* 2010; Del Negro *et al.* 2011), no consensus exists among researchers in this area. Although inhibitory synaptic transmission is necessary in network-driven rhythmogenesis in mature animal preparations (Smith *et al.* 2007), inspiratory-related activity persists even after inhibitory synaptic transmission is blocked in rhythmically active slices (Shao & Feldman, 1997). It is also reported that rhythmogenesis requires subthreshold currents, such as persistent sodium current (I_{NaP}) or non-specific cationic current (I_{CAN}) (Del Negro *et al.* 2005). However, even if both I_{NaP} and I_{CAN} were abolished, the rhythm could be maintained by boosting neural excitability, suggesting that pacemaker neurons are not essential for rhythmogenesis (Del Negro *et al.* 2005). These experimental results suggest the involvement of a currently unknown regulatory factor.

Recent progresses of glial cell physiology has revealed that astrocytes play active roles in various brain functions by driving neuronal synchronization (Parri *et al.* 2001; Angulo *et al.* 2004; Fellin *et al.* 2004; Tian *et al.* 2005). Hülsmann *et al.* (2000) reported that blockade of astrocytic metabolism abolishes inspiratory-related neural output in rhythmically active slices, suggesting that astrocytic metabolic support is necessary for the maintenance of respiratory rhythm. Also, it has been indicated that astrocytes play chemosensory, modulatory and regulatory roles in the respiratory network in the medulla oblongata (Neusch *et al.* 2006; Szoke *et al.* 2006; Ballanyi *et al.* 2010; Erlichman *et al.* 2010; Gourine *et al.* 2010; Huxtable *et al.* 2010; Wenker *et al.* 2010; Gourine & Kasparov, 2011; Mulkey & Wenker, 2011). Härtel *et al.* (2009) showed that astrocytes in the ventral respiratory group are activated by neuromodulators that also stimulate respiratory neurons, suggesting that thus modulated astrocytes influence respiratory neurons in the ventral respiratory group. In humans, abnormalities of brainstem astrocytes correlate with disturbances in central respiratory control, e.g. abnormal proliferation of brainstem astrocytes with central neurogenic hyperventilation (Rodriguez *et al.* 1982) and immaturity of brainstem astrocytes with sudden infant death syndrome (Zhang *et al.* 1992).

These reports led us to further investigate the role of astrocytes in respiratory control, and we conducted large-scale simultaneous analyses of inspiratory-related activities of putative neurons and astrocytes in rhythmically active slices. Here we show that a subset of putative astrocytes in the preBötC is activated preceding inspiratory neuronal firing.

Methods

Animal experiment ethics

All experiments were performed with the approval of the Animal Experiment Ethics Committee at the University of Tokyo (approval numbers: 19-35 and 19-43) and were in accordance with the University of Tokyo guidelines for the care and use of laboratory animals.

Preparations

Rhythmically active slices were prepared from rats for calcium imaging ($n = 16$) or from mice for optogenetic experiments ($n = 30$) between postnatal days 1 and 3. Briefly, animals were deeply anaesthetized with diethyl ether, and the brainstem was dissected and mounted with its rostral side down on an agar block, and transferred to a vibratome (VT1200S, Leica, Heidelberg, Germany). The brainstem was serially sectioned until the most caudal portion of the inferior olive, which approximately corresponded to the third or fourth hypoglossal nerve rootlet. Then a transverse slice containing the preBötC was prepared with a thickness of 550–650 μm. The rostral surface of the slice should coincide with the rostral end of the preBötC or be within approximately 50 μm rostral to the preBötC (see Fig. 1*A* in Ruangkittisakul *et al.* (2008)). The slice was placed in a submerged-type recording chamber with its rostral side up, and continuously superfused with oxygenated (95% O_2 and 5% CO_2) artificial cerebrospinal fluid (aCSF) containing (in mM): 118 NaCl, 3 KCl, 1.2 $CaCl_2$, 1 $MgCl_2$, 1 NaH_2PO_4, 25 $NaHCO_3$ and 30 D-glucose (~330 mosmol l^{-1}, pH 7.4). The temperature was maintained at 28°C. The concentration of potassium

ions was then elevated to 8 mM to activate and maintain rhythmic activity (Smith *et al.* 1991).

Calcium imaging

A glass pipette (1–3 MΩ) for dye loading was filled with aCSF containing of 200 μM Oregon Green 488 BAPTA-1 AM (OGB1, Invitrogen, Carlsbad, CA, USA), 2% Pluronic F-127 (Invitrogen) and 20% DMSO. The tip of the pipette was inserted into the centre of the preBötC region of rhythmically active slices. The point of pipette insertion was carefully determined making reference to Fig. 2*C* of Ruangkittisakul *et al.* (2009). Then, the dye solution was pressure-ejected over 3–5 min by manually controlling a 10 ml syringe press (30–70 kPa), following the calcium dye injection technique originally developed for the use *in vivo* (Stosiek *et al.* 2003) and later applied to the preBötC *in vitro* by the group of Ballanyi (Ruangkittisakul *et al.* 2006, 2008). The fluorophore was excited at 488 nm using a laser diode (2–8 mW, HPU50101, FITEL, Tokyo, Japan) and was recorded through a 507 nm long-pass emission filter. Images (512 × 512 pixels = 512 × 512 μm, 14-bit intensity) were captured at 5–50 frames s^{-1} using a Nipkow-disk confocal scanner unit (CSU-X1; Yokogawa Electric, Tokyo, Japan), a back-illuminated cooled CCD camera (iXon DU897; Andor, Belfast, Northern Ireland, UK), an upright microscope (ECLIPSE FN1; Nikon, Tokyo, Japan) and a water-immersion objective lens (16×, 0.8 NA or 40×, 0.8 NA, Nikon).

Analysis of calcium dynamics

First, a region covering the whole preBötC was set in order to show average calcium rises in the entire preBötC. Second, a small region of interest (ROI) was carefully placed on (within) each recorded cell body, and the fluorescence intensity (F) was measured. In some cases, non-cellular structures were labelled with calcium dyes, and thus we carefully avoided placing ROIs on these structures based on the following two features. First, because the somata of cells are separated at a cell-to-cell distance at least 20 μm, the ROIs were not placed within 20 μm from the nearest ROI. Second, each ROI was set to be 50–75 μm^2 in size to avoid placing ROIs on the small non-cellular structures. Some astrocytes contact vessels through their endfeet, and these endfeet were easily identified by eye and excluded from the analysis. In each ROI, the fluorescence intensity was spatially averaged. The change in fluorescence ($\Delta F/F$) in a ROI was calculated as $(F_t - F_0)/F_0$, where F_t was the fluorescence intensity at a focused time point and F_0 was the average baseline fluorescence intensity across the 10 s periods before and after the focused time point. No image compensation was made to cancel background inspiratory activity.

Functional classification of neurons and astrocytes

In calcium imaging experiments, recorded cells were often classified into neurons and astrocytes on the basis of distinct calcium rise patterns, i.e. faster and slower calcium rises in neurons and astrocytes, respectively (e.g. Pasti *et al.* 1997; Fellin *et al.* 2004, 2006; Bardoni *et al.* 2010). In the present study, however, we intended to classify the recorded cells into putative neurons and putative astrocytes more reliably, and conducted principal component analysis of the waveforms derived from the cellular calcium dynamics. The $\Delta F/F$ waveform was quantified with the following multivariate measures: the rise time constant, maximum rise amplitude and decay time constant of fluorescent calcium signals, based on the universally observed characteristics that the astrocytic calcium changes exhibit slower kinetics and higher amplitude rises compared with those of neurons (Pasti *et al.* 1997; Svoboda *et al.* 1997; Garaschuk *et al.* 2000; Parri *et al.* 2001; Stosiek *et al.* 2003; Fellin *et al.* 2004, 2006; Hirase *et al.* 2004; Nimmerjahn *et al.* 2004; Sasaki *et al.* 2007, 2011*a*; Bardoni *et al.* 2010; Takahashi *et al.* 2010). The dataset was decomposed into a lower dimensional space of the first two components of the principal component analysis, a linear data-reduction technique (Sasaki *et al.* 2008). The first two principal components were plotted in a figure. The calcium dynamics were automatically classified using a linear support-vector machine. The support-vector machine is one of the most widely used supervised learning methods for classification, initially conceived by Cortes & Vapnik (1995). Further, cell sizes and an identity factor were incorporated. The identity factor scores +1 or −1, according to subjective judgement of neurons or astrocytes based on their calcium waveforms and soma sizes (assuming soma diameter <10 μm as astrocyte and soma diameter >10 μm as neuron) (Ruangkittisakul *et al.* 2009; Huxtable *et al.* 2010) were used for *post hoc* confirmation of the cell types after automatic classification. Cells were thus classified into putative neurons and putative astrocytes, and this classification was validated in a selected sample by S100β immunoreactivity and by their responses to tetrodotoxin (see Results).

Classification of astrocyte types

Based on the relative timings of astrocytic activity to inspiratory neuronal activity, recorded putative astrocytes were classified into four types: preinspiratory cells (type 1), inspiratory cells (type 2), non-respiratory cells (type 3) and silent cells (type 4). Preinspiratory cells were defined

as cells that were activated 0.5–2 s earlier than inspiratory neuronal activity. Inspiratory cells were defined as cells that were activated corresponding with inspiratory timings. Non-inspiratory cells were defined as cells that were activated irrespective of inspiratory timings. Silent cells were defined as cells that were not activated at least during our recording period of 5 min.

Electrophysiology

All electrophysiological recordings were carried out with a MultiClamp 700B amplifier and a Digidata 1440A digitizer controlled by pCLAMP 10 software (Molecular Devices, Union City, CA, USA). Spontaneous multi-unit activity was recorded from the preBötC using borosilicate glass pipettes (~1 MΩ) and integrated along a time window of 300 ms (Funke *et al.* 2007). This integrated signal of spontaneous multi-unit activity has been widely used as neural output of inspiratory activity (Funke *et al.* 2007; Ruangkittisakul *et al.* 2009; Schnell *et al.* 2011). The onset of integrated signal faithfully coincided with that of average fluorescence signal recorded from the entire preBötC region, and thus the average fluorescence signal was used as an alternative of electrophysiologically recorded inspiratory neural output. For cell-attached recordings, borosilicate glass pipettes (4–7 MΩ) were filled with aCSF. For current-clamp recordings, the same pipettes were filled with an internal solution consisting of (in mM): 135 potassium gluconate, 4 KCl, 10 HEPES, 10 phosphocreatine-Na_2, 0.3 Na_2-GTP and 4 Mg-ATP (pH 7.2). Signals were low-pass filtered at 1–2 kHz, digitized at 10 kHz and analysed with pCLAMP 10 software.

Optogenetics

Megalencephalic leukoencephalopathy with subcortical cysts (MLC) is a neurological disorder caused by mutations in the MLC1 gene in human. MLC1 and its mouse homologue, Mlc1, are specifically expressed in astrocytes (Schmitt *et al.* 2003). To selectively excite astrocytes, we developed transgenic mice that expressed the light-activated ion channel, channelrhodopsin-2 (ChR2), fused to enhanced yellow fluorescent protein (YFP), under the control of the astrocyte-specific Mlc1 gene promoter. The ChR2(C128S mutant)–YFP fusion molecule, a gift from Karl Deisseroth (Berndt *et al.* 2009), was selectively expressed in astrocytes using the tetracycline transactivator (tTA)–tetO promoter strategy (Gossen *et al.* 1995), whereby two lines of mice were bred, one expressing an astrocyte-specific promoter driving tTA expression and the other expressing the tetO promoter driving the ChR2–YFP transgene. The transgene was induced by binding of tTA to tetO. Mlc1-tTA mice (Tanaka *et al.* 2010) expressing tTA under the control of the astrocyte specific gene (Mlc1) promoter were bred with the newly developed tetO-ChR2(C128S)–YFP mice (Tanaka *et al.* in press). ChR2 is a cation-selective membrane channel, and by photo-activation it rapidly opens to form a pore permeable to monovalent (Na^+, K^+ and H^+) and divalent (Ca^{2+}) cations (Figueiredo *et al.* 2011). To show the rapid channel opening in photo-stimulated astrocytes, photo-induced inward currents were recorded in patch-clamped astrocytes. As light activation of ChR2 could not be combined with fluorescent OGB1 imaging due to optical interference, inspiratory-related neural activity was electrophysiologically monitored from the preBötC. Since our experiments with photo-activation of astrocytes aimed to examine whether photo-activation induces neuronal firing and also preliminary experiments indicated that suppression of spontaneous inspiratory-related activity was more advantageous to obtain clearer responses, after we observed spontaneous firings of inspiratory neurons we lowered the superfusate potassium concentration from 8 mM to 4 mM that induced '*in vitro* apnoea' (Smith *et al.* 1991). While a preBötC neuron from a rhythmically active slice was current-clamped, the centre part of the preBötC region, which was determined by referring to Ruangkittisakul *et al.* (2011), was illuminated with a circular spot (diameter ~350 μm) of blue (488 nm; 6.6 mW) or green (540 nm; 19.5 mW) light to selectively stimulate and suppress the preBötC astrocytes for 3–4 s, respectively.

Immunostaining

Functional classification of cells recorded by calcium imaging into neurons and astrocytes was validated in a representative rhythmically active slice of rat by *post hoc* immunoreactivity analysis of S100β, which is an established astrocyte-specific marker protein in rodents (Huxtable *et al.* 2010; Aoyama *et al.* 2011; Sasaki *et al.* 2011*a*), though not necessarily astrocyte-specific in humans (Steiner *et al.* 2007). Also, ChR2–YFP-positive cells in rhythmically active slices of mouse were immunohistochemically examined to determine whether they were exclusively astrocytes.

A rhythmically active slice was fixed as a whole in 4% paraformaldehyde in 0.1 M phosphate buffer solution overnight at 4°C and permeabilized and blocked with 0.1% Triton X-100 and 5% goat serum at room temperature (Sasaki *et al.* 2011*a*). It was then incubated overnight with primary mouse monoclonal anti-S100β antibody (S2532, Sigma-Aldrich, 1:1000) and 1 μg ml^{-1} affinity-purified rabbit antibody to green fluorescent protein (gift from Takeshi Kaneko; Tamamaki *et al.* 2000) and labelled with secondary anti-rabbit IgG Alexa-488 (A11008, Invitrogen, 1:500), anti-mouse IgG Alexa-594 (A11032, Invitrogen, 1:500) and Neuro Trace 435/455

blue fluorescent Nissl (N21479, Invitrogen, 1:50), which specifically stains neuronal somata (Schmued *et al.* 1982), for 5 h at room temperature. The region where calcium imaging was conducted was identified based on the structural characteristics of the slice and the distribution of S100β-positive cells in the region that was presumed to be at the same depth as calcium imaging was observed under a confocal microscope (MRC-1024, Bio-Rad, CA, USA).

Results

Inspiratory-related activity patterns of astrocytes and neurons

The medullary region into which OGB1 was bolus-injected emitted green fluorescence, and coincided well with the preBötC in rhythmically active slices of rats (Fig. 1*A*). All tested slices spontaneously exhibited intermittent elevations of total fluorescence intensity in the dye-loaded region, the onset of which faithfully coincided with that of extracellularly recorded inspiratory neuron bursting, as previously shown (Koshiya & Smith, 1999; Ruangkittisakul *et al.* 2009) (Fig. 1*B*). These inspiratory-related rhythmic signals were monitored at 5–50 frames s^{-1} at a cellular resolution using a Nipkow-disk confocal microscope. Single videos were 243 ± 14 s in length, and included 161 ± 23 cells (120 ± 17 putative neurons; 41 ± 5 putative astrocytes) ($n = 25$ videos from 14 slices). The recorded cells were classified into putative astrocytes and putative neurons by principal component analysis of the waveforms derived from the cellular calcium dynamics and of the cell sizes (Fig. 1*C*). This functional cell classification was validated by *post hoc* immunohistochemical staining for the astrocytic marker S100β (Fig. 1*D*). Cell-attached patch-clamp recordings from these identified cells confirmed that the calcium elevations in putative neurons, but not in putative astrocytes, were associated with action potentials (9.5 ± 5.8 spikes per neuron in one inspiratory phase), thereby validating our classification methodology (Fig. 1*E*;

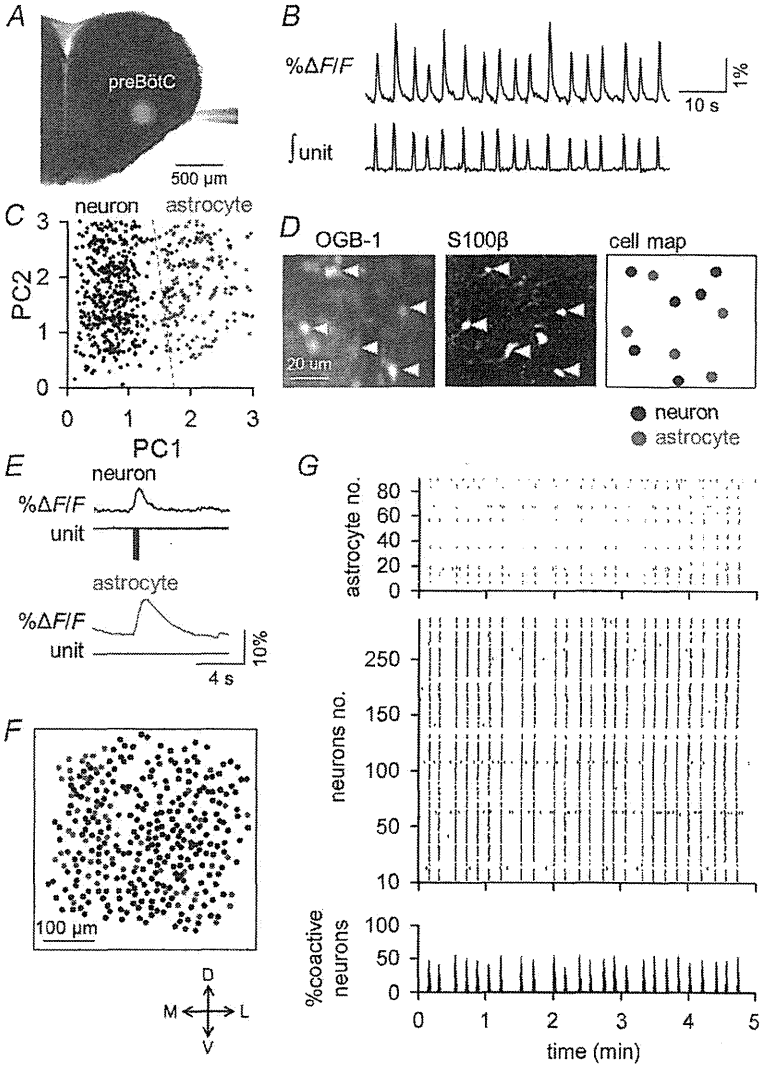

Figure 1. Large-scale multi-cell calcium imaging from the preBötC
A, bolus injection of OGB1 (green) into the preBötC of a rhythmically active slice. *B*, spontaneous fluctuations in the mean fluorescence of the preBötC (top) correlated with the integrated inspiratory unit activity (bottom). *C*, Functional classification of neurons and astrocytes by a principal component (PC) analysis of the calcium waveforms. Putative neurons and putative astrocytes are indicated in black and blue, respectively. *D*, Immunohistochemical classification of neurons and astrocytes (right) based on S100β immunoreactivity (middle) after OGB1 imaging (left). *E*, simultaneous calcium imaging ($\Delta F/F$) and cell-attached recording (unit) from a neuron (top) and an astrocyte (bottom). *F*, locations of 236 putative neurons and 90 putative astrocytes identified in a single video. *G*, raster plots of the calcium activity of the putative astrocytes and putative neurons that are represented in *F*. The bottom histogram indicates the percentage of coactivated putative neurons at a given time (bin = 0.2 s). Putative astrocytes and putative neurons are plotted as blue and black dots, respectively.

putative neuron, $n = 8$ cells; putative astrocyte, $n = 8$ cells). Also, any cells classified as putative neurons did not show spontaneous calcium rises in the presence of tetrodotoxin, which further validated our cell classification (data not shown).

The spatial distribution and spatiotemporal activity patterns of 236 putative neurons and 90 putative astrocytes from one experiment are illustrated in Fig. 1*F* and *G*, respectively. The inspiratory-related modulation of calcium activity was evident in the putative neuronal populations, with a rhythm frequency of 0.16 ± 0.05 Hz and with $55 \pm 19\%$ of putative neurons participating in a single respiratory cycle ($n = 14$ videos).

Activity of putative astrocytes precedes inspiratory neuronal firing

A fraction of putative astrocytes also exhibited inspiratory-related modulation of their calcium activity in slices of rats (Fig. 1*G*). Thus, we analysed the temporal profile of the individual putative astrocytic responses. Trace plots of the inspiratory-related activity revealed that a subset of putative astrocytes were activated early relative to the inspiratory neuronal activity with a time lag of approximately 2 s (Fig. 2*A* and *B* and Supplementary video). The location of these preinspiratory putative astrocytes was unlikely to indicate spatial organization (Fig. 2*C*). In the present study, 10.5% of putative astrocytes were found to be preinspiratory, 3.2% of cells exhibited spontaneous calcium activity irrespective of inspiratory-related activity and 86.3% were either inspiratory or silent during the observation period. We avoided strict separation of inspiratory and silence cells when counting their numbers, because recorded cell activity could reflect a small contamination with background inspiratory fluorescence of neuropiles (Fig. 2*D*).

Intrinsic rhythmic activity of preinspiratory putative astrocytes

To analyse activity patterns of putative astrocytes without the influence of neuronal firings, we blocked neuronal activity by bath application of 1 μM tetrodotoxin, a voltage-sensitive Na^+ channel inhibitor in slices of

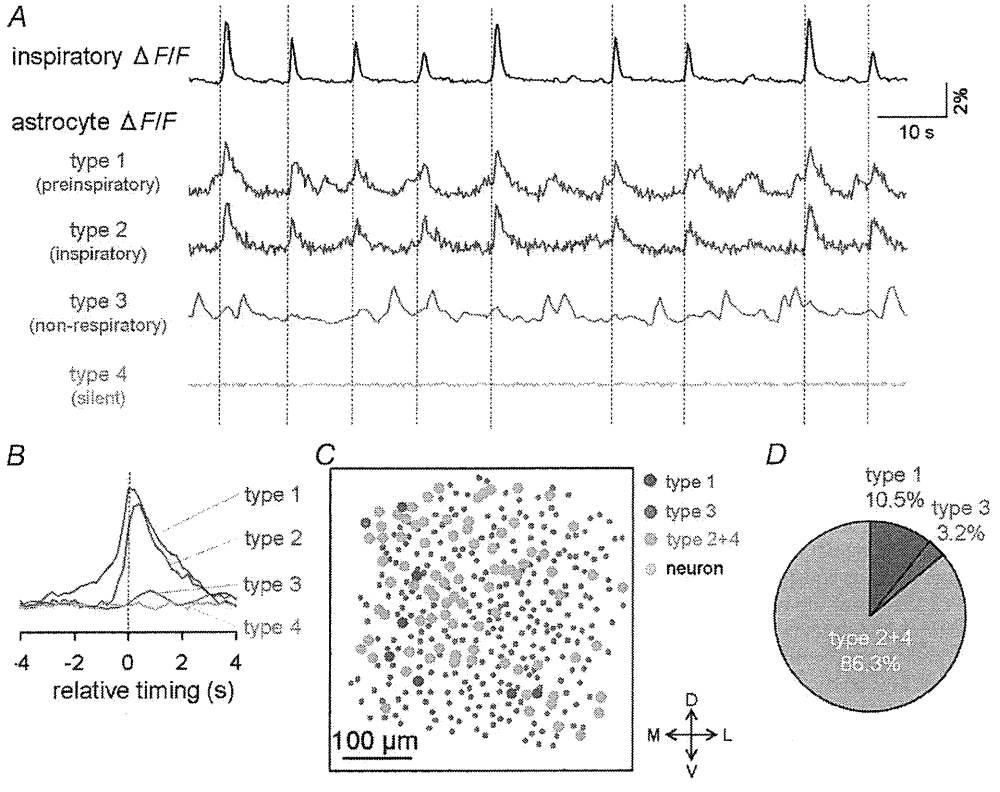

Figure 2. Preinspiratory activity of putative astrocytes
A, representative calcium $\Delta F/F$ traces of preinspiratory (type 1), inspiratory (type 2), non-respiratory (type 3) and silent putative astrocytes (type 4). Top: bulk $\Delta F/F$ fluctuations of the preBötC. *B*, peri-inspiratory $\Delta F/F$ responses of preinspiratory, inspiratory, non-respiratory and silent putative astrocytes. The traces were averaged from 20 successive events by aligning the onset of individual inspiratory events at 0 s. *C*, representative cell map of putative neurons and four types of putative astrocytes. We avoided strict separation of inspiratory and silence cells, and they are shown together as type 2+4. *D*, distribution of four types of putative astrocytes ($n = 541$ putative astrocytes from 14 movies).

rats. Preinspiratory and inspiratory putative astrocytes maintained their periodic calcium rises even during the blockade of neuronal activity with tetrodotoxin, whereas the intercellular phases of these rhythmic activities were decoupled (Fig. 3*A*). Tetrodotoxin also reduced the frequency of calcium rises in preinspiratory, inspiratory and non-respiratory putative astrocytes (Fig. 3*B*). The activity patterns of the preinspiratory and inspiratory putative astrocytes tended to be more periodic than that of non-respiratory putative astrocytes both before and after application of tetrodotoxin, although their differences were not statistically significant when their rhythm regularities were assessed by the coefficient of variation (CV) in inter-activity intervals (Fig. 3*C*). The regularity of rhythmic activity of preinspiratory putative astrocytes was similar to that of inspiratory neuronal activity (Fig. 3*C*). It was interesting to find that tetrodotoxin induced rhythmic calcium activity with unknown mechanisms in a small number of putative astrocytes that were silent before application of tetrodotoxin (bottom trace in Fig. 3*A*).

Selective photo-stimulation of preBötC astrocytes

To gain an insight into the functional role of preBötC astrocytes, we examined whether astrocytes in the preBötC were capable of activating inspiratory neurons, by selectively photo-stimulating astrocytes in the centre part of the preBötC in slices of ChR2(C128S)–YFP transgenic mice (Fig. 4*A*). As ChR2 is rapidly inactivated after cessation of light application, we employed the C128S point mutation of ChR2 (Berndt *et al.* 2009), which alters the photocycle, enabling bistable, step-like control of cell membrane potentials by two different wavelengths. This optical property is effective to mimic the slow kinetics (2–4 s) of astrocytic calcium dynamics. To confirm the specificity of transgene expression in astrocytes, we performed simultaneous Nissl staining that specifically stains neuronal somata and immunohistochemistry for YFP and for an astrocyte-specific marker S100β (Fig. 4*B*). In the preBötC, 45% of S100β-positive cells expressed YFP signals ($n = 278$ cells from 16 slices). On the other hand, there was no overlap between Nissl-positive cells and YFP signals ($n = 895$ cells from 16 slices). To further validate the specificity of transgene expression, whole-cell patch-clamp recordings were performed randomly from astrocytes and neurons in the presence of 1 μM tetrodotoxin, 100 μM Cd^{2+} and 50 μM 6-cyano-7-nitroquinoxaline-2,3-dione (CNQX) to avoid generation of action potentials, Ca^{2+}-dependent vesicular releases and non-NMDA receptor-mediated transmission,

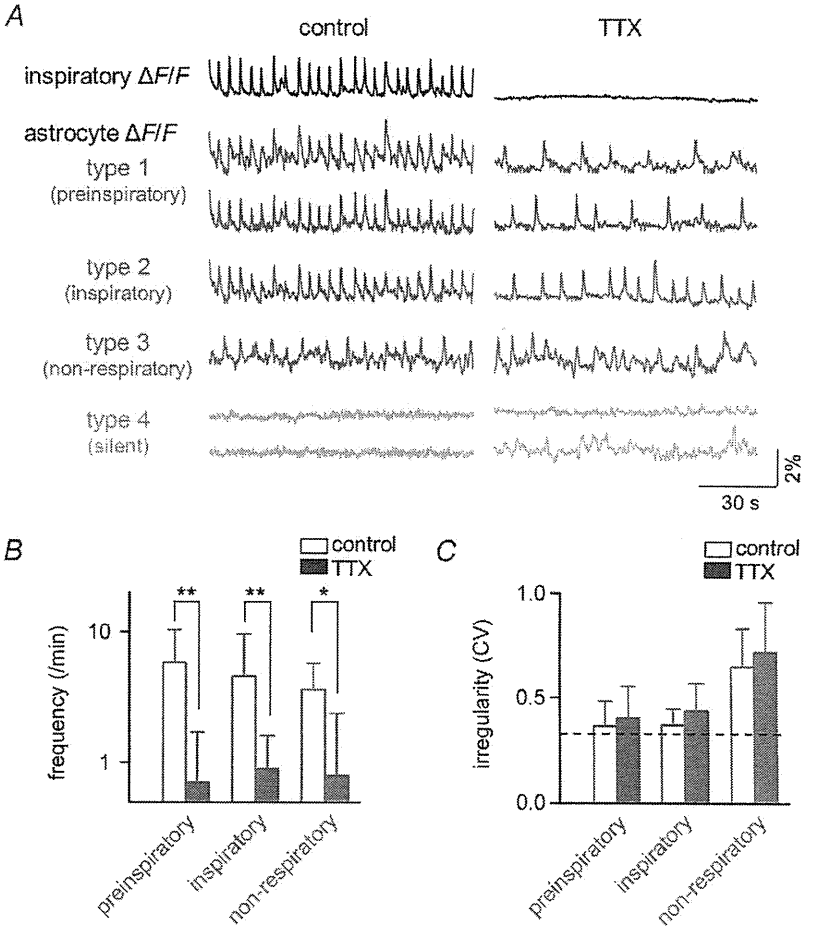

Figure 3. Intrinsic rhythmic activities of preinspiratory putative astrocytes
A, representative overall inspiratory $\Delta F/F$ traces (top) and calcium $\Delta F/F$ traces of preinspiratory, inspiratory, non-respiratory and silent putative astrocytes before and after application of tetrodotoxin. Note that the bottom silent trace exhibits activity after application of tetrodotoxin. *B*, the mean frequency of calcium events in preinspiratory (blue, $n = 20$ cells), inspiratory (red, $n = 175$ cells) and non-respiratory putative astrocytes (green, $n = 14$ cells) in the presence (filled bar) or absence (open bar) of tetrodotoxin. *C*, coefficient of variation (CV) of the time-intervals between two successive calcium events in preinspiratory, inspiratory and non-respiratory putative astrocytes in the presence or absence of tetrodotoxin. The dashed line indicates the CV of the inspiratory-related neuronal activity in the presence of tetrodotoxin, i.e. the irregularity of the inspiratory rhythm. $^*P < 0.05$, $^{**}P < 0.01$, paired *t* test.

respectively, if any. In astrocytes, 5 out of 9 cells exhibited inward currents in response to brief illumination with blue light, and the currents persisted until flashed with green light (Fig. 4*C*, top). The average amplitude of the photocurrents was 68 ± 37 pA ($n = 5$ astrocytes). In contrast, no current responses to photo-stimulation were observed in all neurons tested ($n = 25$ cells) (Fig. 4*C*, bottom). These histological and electrophysiological findings clearly demonstrate that ChR2(C128S)–YFP was expressed exclusively in a subset of astrocytes. Using this transgenic mouse line, we then investigated the effect of selective activation of preBötC astrocytes on excitability of neighbouring inspiratory neurons. Photo-activation of astrocytes elicited single or burst firing of action potentials in 8 of 16 preBötC inspiratory neurons in the ChR2(C128S)–YFP transgenic mice ($n = 16$ mice), but not in the wild-type mice ($n = 9$ cells from 9 mice) (Fig. 4*D* and *E*). In the eight responsive neurons, 75 ± 11% of trials with light stimulation elicited action potentials (Fig. 4*F*) and the latency from the stimulus onset to the first spike was 5.5 ± 0.9 s (Fig. 4*G*).

Discussion

In the present study we have shown that a subset of putative astrocytes exhibited calcium elevations preceding inspiratory neuronal activity with a time lag of approximately 2 s. These preinspiratory putative astrocytes maintained their rhythmic activity even during the blockade of neuronal activity with tetrodotoxin, whereas their rhythm frequency was lowered and the intercellular phases of these rhythms were decoupled. Optogenetic stimulation of preBötC astrocytes induced firing of inspiratory neurons.

Recently, a number of studies by calcium imaging in the preBötC have been reported. However, none showed respiratory-related rhythmic calcium activity in astrocytes (e.g. Funke *et al.* 2007; Härtel *et al.* 2009; Ruangkittisakul *et al.* 2009), and the present study is the first to show respiratory-related stable rhythmic calcium activities in putative astrocytes. Therefore, the preinspiratory activity in putative astrocytes is also first reported here. Although it is not clear why respiratory-related rhythmic calcium activities in astrocytes have not previously been reported; it may be partly attributed to the experimental technique

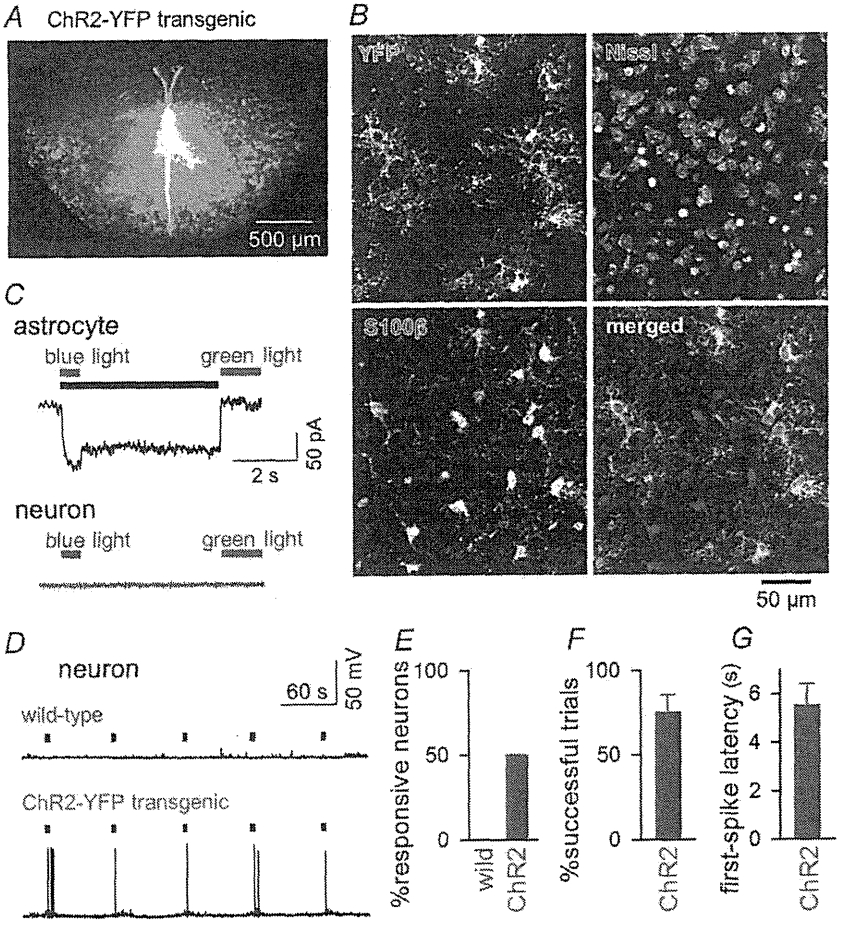

Figure 4. Astrocyte-driven action potentials in inspiratory neurons
A, YFP fluorescence of a rhythmically active slice prepared from a Mlc1-tTA::tetO-ChR2(C128S)–YFP transgenic mouse. *B*, triple labelling of preBötC cells with an antibody against green fluorescent protein (i.e. YFP appearing in green) to indicate ChR2-expressing cells, with fluorescent Nissl to show neuronal somata (blue), and with an antibody against S100β to identify astrocytes (red). ChR2–YFP positivity was found exclusively in S100β-positive cells. Thus, ChR2 was expressed only in astrocytes. *C*, switch-on (blue light) and switch-off (green light) of a persistent inward current in a voltage-clamped ChR2-expressing astrocyte (top) and neuron (bottom). Voltages were clamped at −70 mV. The black bar indicates the activated period. *D*, photo-activation of astrocytes triggers action potentials in an inspiratory neuron from the preBötC in a ChR2(C128S)YFP transgenic (but not in a wild-type) mouse. Black bars indicate the activation periods of preBötC astrocytes. *E*, ratios of neurons that fired in response to photo-activation of astrocytes in wild-type ($n = 9$ neurons) and in ChR2(C128S)YFP transgenic mice ($n = 16$ neurons from 5 animals). *F*, ratios of the trials in which light stimulation elicited action potentials ($n = 8$ responsive neurons). *G*, latency from the light-stimulus onset to the first spike ($n = 8$ neurons).

in previous studies, i.e. calcium indicator dyes were injected into the midline of the slice to selectively label neurons through axons of passage (Koizumi *et al.* 2008; Koshiya & Smith, 1999), imaging areas were rather small (Koizumi *et al.* 2008) or injected dyes preferentially stained neurons. On the contrary, we directly stained the preBötC region and conducted large-scale imaging, and the dye we used, OGB1, appears to preferentially stain astrocytes (Funke *et al.* 2007; Sasaki *et al.* 2011*a*). Recently, Schnell *et al.* (2011) analysed functional coupling between astrocytes and neurons, detected a rhythmic inwardly directed current that was entrained to neuron population discharges in 10% of preBötC astrocytes by whole-cell patch recording, and attributed the rhythmic current fluctuation to periodic elevations of extracellular potassium that were produced by efflux from rhythmically oscillating neurons and to consequent changes in potassium equilibrium potentials of astrocytes (Brockhaus *et al.* 1993; Okada *et al.* 2005). However, Schnell *et al.* (2011) did not detect periodic calcium rises in astrocytes coupled with neuronal rhythmic activities. Although they observed spontaneous calcium fluctuation in astrocytes, it did not propagate to or from other cells. To explain the discrepancy between their and our observations, further studies are needed.

Optogenetic stimulation is a powerful method to study the function of astrocytes (Figueiredo *et al.* 2011). It has been reported that optogenetic stimulation of chemosensory astrocytes near the ventral surface of the medulla oblongata induces respiratory augmentation (Gourine *et al.* 2010). In the present study we applied an optogenetic stimulation technique, and carefully focused the photo-stimulating region within the the preBötC. Thus, chemosensory astrocytes near the ventral surface should not have been excited. Although we could induce inspiratory neuronal firings by optogenetic stimulation of astrocytes in the preBötC, not only preinspiratory but all other types of astrocytes expressing ChR2 should have been excited with this technique. Also, the latency approximately 5 s after photo-stimulation to inspiratory neuronal firings, as well as the latency approximately 2 s after activation of preinspiratory putative astrocytes to inspiratory neuronal firings, appear too long, if assuming a pacemaking role in preinspiratory astrocytes to trigger inspiratory neurons especially in *in vivo* conditions where breathing rates are notably faster than 1 Hz in rodents. Further studies are necessary to examine the response of inspiratory neurons to selective activation of preinspiratory astrocytes and to clarify the role of astrocytes in respiratory control in *in vitro* and *in vivo* conditions.

Even if preinspiratory astrocytes play an active role in initiating inspiratory neuron firings, the notion does not necessarily contradict any previously proposed neuronal pacemaker or neuronal group pacemaker hypotheses (Koshiya & Smith, 1999; Feldman & Del Negro, 2006; Pace *et al.* 2007; Mironov, 2008; Del Negro *et al.* 2011). Although calcium influxes in the somata of inspiratory neurons have been shown to be a consequence of membrane depolarization and through a voltage-dependent calcium channels (Morgado-Valle *et al.* 2008), those in the dendrites precede somatic inspiratory activity with a time lag of a few hundred milliseconds (Mironov, 2008; Del Negro *et al.* 2011). According to the group pacemaker hypothesis, preBötC excitatory interneurons mutually interact to elevate dendritic calcium, activate I_{CAN} and periodically trigger inspiration (Mironov, 2008; Rubin *et al.* 2009). Our findings raise an alternative possibility that the preinspiratory dendritic calcium elevation and depolarization are evoked, at least partly, by the preceding astrocytic activity (Sasaki *et al.* 2011*b*). Our observation that blockade of neuronal activity with tetrodotoxin slowed and decoupled the periodic calcium rises of preinspiratory putative astrocytes suggests that the neuronal network facilitates the occurrence of calcium transient of preinspiratory astrocytes and synchronizes them. Inspiratory neurons appear to have an influence on the rhythmic glial activities and thus preinspiratory astrocytes and inspiratory neurons seem to have mutual interactions in the preBötC.

These findings, together with previous reports that inhibition of astrocytic metabolism abolishes inspiratory-related neural output in rhythmically active slices (Hülsmann *et al.* 2000) and decreases respiratory frequency in *in vivo* rat pups (Young *et al.* 2005), raise the possibility that astrocytes are actively involved in respiratory rhythm generation in the preBötC. As astrocyte-driven neural synchronization has been reported in many other brain regions (Parri *et al.* 2001; Angulo *et al.* 2004; Fellin *et al.* 2004; Tian *et al.* 2005), we propose a hypothesis that preinspiratory astrocytes are actively involved in respiratory rhythm generation at least in rhythmically active slices. This issue must be thoroughly investigated in the future, in a precisely 'calibrated' rhythmically active slice that can generate an eupnoea-like inspiratory burst pattern in a more physiological superfusate potassium concentration (Ballanyi & Ruangkittisakul, 2009) and by experiments including long-term calcium imaging and patch-clamp recording from astrocytes that are identified, e.g. genetically (e.g. Härtel *et al.* 2009; Ruangkittisakul *et al.* 2009). Also, pharmacological modulation of the bursting rhythm by glial toxins and agonist/antagonist of possible gliotransmitter receptors must be thoroughly examined to clarify whether preinspiratory calcium rise in astrocytes leads inspiratory neuronal firings.

References

Angulo MC, Kozlov AS, Charpak S & Audinat E (2004). Glutamate released from glial cells synchronizes neuronal activity in the hippocampus. *J Neurosci* **24**, 6920–6927.

Aoyama R, Okada Y, Yokota S, Yasui Y, Fukuda K, Shinozaki Y, Yoshida H, Nakamura M, Chiba K, Yasui Y, Kato F & Toyama Y (2011). Spatiotemporal and anatomical analyses of P2X receptor-mediated neuronal and glial processing of sensory signals in the rat dorsal horn. *Pain* **152**, 2085–2097.

Ballanyi K & Ruangkittisakul A (2009). Structure-function analysis of rhythmogenic inspiratory pre-Bötzinger complex networks in 'calibrated' newborn rat brainstem slices. *Respir Physiol Neurobiol* **168**, 158–178.

Ballanyi K, Panaitescu B & Ruangkittisakul A (2010). Control of breathing by 'nerve glue'. *Sci Signal* **3**, pe41.

Bardoni R, Ghirri A, Zonta M, Betelli C, Vitale G, Ruggieri V, Sandrini M & Carmignoto G (2010). Glutamate-mediated astrocyte-to-neuron signalling in the rat dorsal horn. *J Physiol* **588**, 831–846.

Berndt A, Yizhar O, Gunaydin LA, Hegemann P & Deisseroth K (2009). Bi-stable neural state switches. *Nat Neurosci* **12**, 229–234.

Brockhaus J, Ballanyi K, Smith JC & Richter DW (1993). Microenvironment of respiratory neurons in the *in vitro* brainstem–spinal cord of neonatal rats. *J Physiol* **462**, 421–445.

Cortes C & Vapnik V (1995). Support-vector networks. *Mach Learn* **20**, 273–297.

Del Negro CA, Hayes JA & Rekling JC (2011). Dendritic calcium activity precedes inspiratory bursts in preBötzinger complex neurons. *J Neurosci* **31**, 1017–1022.

Del Negro CA, Morgado-Valle C, Hayes JA, Mackay DD, Pace RW, Crowder EA & Feldman JL (2005). Sodium and calcium current-mediated pacemaker neurons and respiratory rhythm generation. *J Neurosci* **25**, 446–453.

Erlichman JS, Leiter JC & Gourine AV (2010). ATP, glia and central respiratory control. *Respir Physiol Neurobiol* **173**, 305–311.

Feldman JL & Del Negro CA (2006). Looking for inspiration: new perspectives on respiratory rhythm. *Nat Rev Neurosci* **7**, 232–242.

Fellin T, Gomez-Gonzalo M, Gobbo S, Carmignoto G & Haydon PG (2006). Astrocytic glutamate is not necessary for the generation of epileptiform neuronal activity in hippocampal slices. *J Neurosci* **26**, 9312–9322.

Fellin T, Pascual O, Gobbo S, Pozzan T, Haydon PG & Carmignoto G (2004). Neuronal synchrony mediated by astrocytic glutamate through activation of extrasynaptic NMDA receptors. *Neuron* **43**, 729–743.

Figueiredo M, Lane S, Tang F, Liu BH, Hewinson J, Marina N, Kasymov V, Souslova EA, Chudakov DM, Gourine AV, Teschemacher AG & Kasparov S (2011). Optogenetic experimentation on astrocytes. *Exp Physiol* **96**, 40–50.

Funke F, Dutschmann M & Müller M (2007). Imaging of respiratory-related population activity with single-cell resolution. *Am J Physiol Cell Physiol* **292**, C508–C516.

Garaschuk O, Linn J, Eilers J & Konnerth A (2000). Large-scale oscillatory calcium waves in the immature cortex. *Nat Neurosci* **3**, 452–459.

Gossen M, Freundlieb S, Bender G, Muller G, Hillen W & Bujard H (1995). Transcriptional activation by tetracyclines in mammalian cells. *Science* **268**, 1766–1769.

Gourine AV & Kasparov S (2011). Astrocytes as brain interoceptors. *Exp Physiol* **96**, 411–416.

Gourine AV, Kasymov V, Marina N, Tang F, Figueiredo MF, Lane S, Teschemacher AG, Spyer KM, Deisseroth K & Kasparov S (2010). Astrocytes control breathing through pH-dependent release of ATP. *Science* **329**, 571–575.

Härtel K, Schnell C & Hülsmann S (2009). Astrocytic calcium signals induced by neuromodulators via functional metabotropic receptors in the ventral respiratory group of neonatal mice. *Glia* **57**, 815–827.

Hirase H, Qian L, Barthó P & Buzsáki G (2004). Calcium dynamics of cortical astrocytic networks *in vivo*. *PLoS Biol* **2**, E96.

Hülsmann S, Oku Y, Zhang W & Richter DW (2000). Metabolic coupling between glia and neurons is necessary for maintaining respiratory activity in transverse medullary slices of neonatal mouse. *Eur J Neurosci* **12**, 856–862.

Huxtable AG, Zwicker JD, Alvares TS, Ruangkittisakul A, Fang X, Hahn LB, Posse de Chaves E, Baker GB, Ballanyi K & Funk GD (2010). Glia contribute to the purinergic modulation of inspiratory rhythm-generating networks. *J Neurosci* **30**, 3947–3958.

Koizumi H & Smith JC (2008). Persistent Na^+ and K^+-dominated leak currents contribute to respiratory rhythm generation in the pre-Bötzinger complex *in vitro*. *J Neurosci* **28**, 1773–1785.

Koizumi H, Wilson CG, Wong S, Yamanishi T, Koshiya N & Smith JC (2008). Functional imaging, spatial reconstruction, and biophysical analysis of a respiratory motor circuit isolated *in vitro*. *J Neurosci* **28**, 2353–2365.

Koshiya N & Smith JC (1999). Neuronal pacemaker for breathing visualized *in vitro*. *Nature* **400**, 360–363.

Mironov SL (2008). Metabotropic glutamate receptors activate dendritic calcium waves and TRPM channels which drive rhythmic respiratory patterns in mice. *J Physiol* **586**, 2277–2291.

Morgado-Valle C, Baca SM & Feldman JL (2010). Glycinergic pacemaker neurons in preBötzinger complex of neonatal mouse. *J Neurosci* **30**, 3634–3639.

Morgado-Valle C, Beltran-Parrazal L, DiFranco M, Vergara JL & Feldman JL (2008). Somatic Ca^{2+} transients do not contribute to inspiratory drive in preBötzinger complex neurons. *J Physiol* **586**, 4531–4540.

Mulkey DK & Wenker IC (2011). Astrocyte chemoreceptors: mechanisms of H^+ sensing by astrocytes in the retrotrapezoid nucleus and their possible contribution to respiratory drive. *Exp Physiol* **96**, 400–406.

Neusch C, Papadopoulos N, Müller M, Maletzki I, Winter SM, Hirrlinger J, Handschuh M, Bähr M, Richter DW, Kirchhoff F & Hülsmann S (2006). Lack of the Kir4.1 channel subunit abolishes K+ buffering properties of astrocytes in the ventral respiratory group: impact on extracellular K^+ regulation. *J Neurophysiol* **95**, 1843–1852.

Nimmerjahn A, Kirchhoff F, Kerr JN & Helmchen F (2004). Sulforhodamine 101 as a specific marker of astroglia in the neocortex *in vivo*. *Nat Methods* **1**, 31–37.

Okada Y, Kuwana S, Kawai A, Mückenhoff K & Scheid P (2005). Significance of extracellular potassium in central respiratory control studied in the isolated brainstem-spinal cord preparation of the neonatal rat. *Respir Physiol Neurobiol* **146**, 21–32.

Pace RW, Mackay DD, Feldman JL & Del Negro CA (2007). Inspiratory bursts in the preBötzinger complex depend on a calcium-activated non-specific cation current linked to glutamate receptors in neonatal mice. *J Physiol* **582**, 113–125.

Parri HR, Gould TM & Crunelli V (2001). Spontaneous astrocytic Ca^{2+} oscillations *in situ* drive NMDAR-mediated neuronal excitation. *Nat Neurosci* **4**, 803–812.

Pasti L, Volterra A, Pozzan T & Carmignoto G (1997). Intracellular calcium oscillations in astrocytes: a highly plastic, bidirectional form of communication between neurons and astrocytes *in situ*. *J Neurosci* **17**, 7817–7830.

Rodriguez M, Baele PL, Marsh HM & Okazaki H (1982). Central neurogenic hyperventilation in an awake patient with brainstem astrocytoma. *Ann Neurol* **11**, 625–628.

Ruangkittisakul A, Okada Y, Oku Y, Koshiya N & Ballanyi K (2009). Fluorescence imaging of active respiratory networks. *Respir Physiol Neurobiol* **168**, 26–38.

Ruangkittisakul A, Panaitescu B & Ballanyi K (2011). K^+ and Ca^{2+} dependence of inspiratory-related rhythm in novel 'calibrated' mouse brainstem slices. *Respir Physiol Neurobiol* **175**, 37–48.

Ruangkittisakul A, Schwarzacher SW, Secchia L, Ma Y, Bobocea N, Poon BY, Funk GD & Ballanyi K (2008). Generation of eupnea and sighs by a spatiochemically organized inspiratory network. *J Neurosci* **28**, 2447–2458.

Ruangkittisakul A, Schwarzacher SW, Secchia L, Poon BY, Ma Y, Funk GD & Ballanyi K (2006). High sensitivity to neuromodulator-activated signaling pathways at physiological $[K^+]$ of confocally imaged respiratory center neurons in on-line-calibrated newborn rat brainstem slices. *J Neurosci* **26**, 11870–11880.

Rubin JE, Hayes JA, Mendenhall JL & Del Negro CA (2009). Calcium-activated nonspecific cation current and synaptic depression promote network-dependent burst oscillations. *Proc Natl Acad Sci U S A* **106**, 2939–2944.

Sasaki T, Kuga N, Namiki S, Matsuki N & Ikegaya Y (2011*a*). Locally synchronized astrocytes. *Cereb Cortex* **21**, 1889–1900.

Sasaki T, Matsuki N & Ikegaya Y (2007). Metastability of active CA3 networks. *J Neurosci* **27**, 517–528.

Sasaki T, Matsuki N & Ikegaya Y (2011*b*). Action-potential modulation during axonal conduction. *Science* **331**, 599–601.

Sasaki T, Takahashi N, Matsuki N & Ikegaya Y (2008). Fast and accurate detection of action potentials from somatic calcium fluctuations. *J Neurophysiol* **100**, 1668–1676.

Schmitt A, Gofferje V, Weber M, Meyer J, Mössner R & Lesch KP (2003). The brain-specific protein MLC1 implicated in megalencephalic leukoencephalopathy with subcortical cysts is expressed in glial cells in the murine brain. *Glia* **44**, 283–295.

Schmued LC, Swanson LW & Sawchenko PE (1982). Some fluorescent counterstains for neuroanatomical studies. *J Histochem Cytochem* **30**, 123–128.

Schnell C, Fresemann J & Hülsmann S (2011). Determinants of functional coupling between astrocytes and respiratory neurons in the pre-Bötzinger complex. *PLoS One* **6**, e26309.

Shao XM & Feldman JL (1997). Respiratory rhythm generation and synaptic inhibition of expiratory neurons in pre-Bötzinger complex: differential roles of glycinergic and GABAergic neural transmission. *J Neurophysiol* **77**, 1853–1860.

Smith JC, Abdala AP, Koizumi H, Rybak IA & Paton JF (2007). Spatial and functional architecture of the mammalian brain stem respiratory network: a hierarchy of three oscillatory mechanisms. *J Neurophysiol* **98**, 3370–3387.

Smith JC, Ellenberger HH, Ballanyi K, Richter DW & Feldman JL (1991). Pre-Bötzinger complex: a brainstem region that may generate respiratory rhythm in mammals. *Science* **254**, 726–729.

Steiner J, Bernstein HG, Bielau H, Berndt A, Brisch R, Mawrin C, Keilhoff G & Bogerts B (2007). Evidence for a wide extra-astrocytic distribution of S100B in human brain. *BMC Neurosci* **8**, 2.

Stosiek C, Garaschuk O, Holthoff K & Konnerth A (2003). *In vivo* two-photon calcium imaging of neuronal networks. *Proc Natl Acad Sci U S A* **100**, 7319–7324.

Svoboda K, Denk W, Kleinfeld D & Tank DW (1997). *In vivo* dendritic calcium dynamics in neocortical pyramidal neurons. *Nature* **385**, 161–165.

Szoke K, Härtel K, Grass D, Hirrlinger PG, Hirrlinger J & Hülsmann S (2006). Glycine transporter 1 expression in the ventral respiratory group is restricted to protoplasmic astrocytes. *Brain Res* **1119**, 182–189.

Takahashi N, Sasaki T, Matsumoto W, Matsuki N & Ikegaya Y (2010). Circuit topology for synchronizing neurons in spontaneously active networks. *Proc Natl Acad Sci U S A* **107**, 10244–10249.

Tamamaki N, Nakamura K, Furuta T, Asamoto K & Kaneko T (2000). Neurons in Golgi-stain-like images revealed by GFP-adenovirus infection *in vivo*. *Neurosci Res* **38**, 231–236.

Tanaka KF, Ahmari SE, Leonardo ED, Richardson-Jones JW, Budreck EC, Scheiffele P, Sugio S, Inamura N, Ikenaka K & Hen R (2010). Flexible Accelerated STOP Tetracycline Operator-knockin (FAST): a versatile and efficient new gene modulating system. *Biol Psychiatry* **67**, 770–773.

Tanaka KF, Matsui K, Sasaki T, Sano H, Sugio S, Fan K, Hen R, Nakai J, Yanagawa Y, Hasuwa H, Okabe M, Deisseroth K, Ikenaka K & Yamanaka A. Expanding the repertoire of optogenetically targeted cells with an enhanced gene expression system. *Cell Reports*, in press.

Tian GF, Azmi H, Takano T, Xu Q, Peng W, Lin J, Oberheim N, Lou N, Wang X, Zielke HR, Kang J & Nedergaard M (2005). An astrocytic basis of epilepsy. *Nat Med* **11**, 973–981.

Wenker IC, Kréneisz O, Nishiyama A & Mulkey DK (2010). Astrocytes in the retrotrapezoid nucleus sense H^+ by inhibition of a Kir4.1-Kir5.1-like current and may contribute to chemoreception by a purinergic mechanism. *J Neurophysiol* **104**, 3042–3052.

Young JK, Dreshaj IA, Wilson CG, Martin RJ, Zaidi SI & Haxhiu MA (2005). An astrocyte toxin influences the pattern of breathing and the ventilatory response to hypercapnia in neonatal rats. *Respir Physiol Neurobiol* **147**, 19–30.

Zhang WD, Tsukamoto T, Yamada Y, Itakura Y, Oono T, Nagao M & Takatori T (1992). Immunohistochemical classification of astrocytes in infants by glial fibrillary acidic protein staining and application to forensic practice. *Nihon Hoigaku Zasshi* **46**, 189–197.

Author contributions

The experiments were performed at the laboratory of Y.I. Y.O.: Conception of the experiments and drafting the article. T.S. and Y.O.: Collection, analysis and interpretation of data and drafting the article. N.T., M.S. and S.U.: Collection of data. K.F.T.: Development of transgenic mice. N.M.: Supervision of experiments and critical revision of the article. Y.I.: Design of the experiments, analysis and interpretation of data, and drafting the article. All authors approved this manuscript.

Acknowledgements

This work was supported in part by Grants-in-Aid for Science Research (nos. 20590218, 22115003, 22650080, 22680025, 23650218, 24300108 and 24500365) from the Ministry of Education, Culture, Sports, Science and Technology of Japan; the Suzuken Memorial Foundation; the Kanae Foundation for the Promotion of Medical Science; the Daiichi-Sankyo Foundation of Life Science; Health and Labour Sciences Research Grants; and the Funding Program for Next Generation World-Leading Researchers (no. LS023). Authors declare no conflict of interest.

SpringerPlus
a SpringerOpen Journal

RESEARCH Open Access

Calcium/calmodulin-dependent protein kinases in the carotid body: an immunohistochemical study

Mieczysław Pokorski[1,2*], Hiroyuki Sakagami[3] and Yasumasa Okada[2]

Abstract

We determined the presence of Ca^{2+}/calmodulin-dependent protein kinases (CaMKs), a family of multifunctional proteins engaged in Ca^{2+}-linked signaling, in carotid body chemoreceptor cells which are critical for the hypoxia-sensing. Carotid bodies were dissected from anesthetized normoxic adult Wistar rats and were double stained for individual CaMKs and for tyrosine hydroxylase (TH), a marker of chemoreceptor cells. Immunofluorescence was examined by confocal laser scanning microscopy. We found that CaMKI and CaMKII were expressed in chemoreceptor cells, but their distribution and intensity varied. CaMKI immunoreactivity was distributed throughout the cytoplasm, whereas that of CaMKII was localized in the cytoplasmic periphery of chemoreceptor cells. An overlap of CaMKI or CaMKII fluorescent probes with TH affirmed the presence of either protein in the chemoreceptor cells. CaMKIV could not be conclusively visualized by the used method. The study shows the expressions of CaMKI and CaMKII in chemoreceptor cells, which raises the plausibility of CaMKs` role in carotid body function.

Keywords: Ca^{2+}/calmodulin-dependent protein kinase, Carotid body, Chemoreceptor cells

Background

Ca^{2+}/calmodulin (CaM)-dependent protein kinases (CaMKs): CaMKI, CaMKII, and CaMKIV are a family of proteins which, through phosphorylation of intracellular substrates, mediate a host of neural functions, including neurotransmitter metabolism, long-term facilitation, and gene transcription. CaMKs are foremost the key regulators of cellular responses to Ca^{2+}/calmodulin mobilizing stimuli (Hook & Means 2001).

Hypoxic hypoxia unleashes pulmonary hyperventilation, a primary reflex defense reaction, aimed at sustaining delivery of O_2 to tissues. The reaction is explicitly generated by the carotid body chemoreceptor cells which detect the deficit of O_2 and transduce that extracellular signal into the intracellular Ca^{2+} rise (Pokorski et al. 2012), followed by neurotransmitter release and a signaling cascade leading eventually to cell excitation and increased neural discharge rate from the organ (Di Giulio et al. 2012; Zara et al. 2012). Ca^{2+} transients are indubitable for the chemoreceptor responses, as these responses are absent after Ca^{2+} chelation (Obeso et al. 1992). CaMKs, fundamentally important proteins for translating transiently evoked Ca^{2+} signals into sustained cellular responses (Hudmon & Schulman 2002), seem well suited to be germane to carotid body function. Indeed, immunoreactivity for CaMKI has been found in the glomus cells, although the exact intracellular location of the enzyme is not well defined (Hoshi et al. 2006). The presence of other CaMKs has never been substantiated in carotid chemoreceptor cells. Therefore, in the present study we endeavored to delineate the expression of individual CaMKs in the normoxic carotid chemoreceptor cells by immunocytochemistry.

Results

We found that CaMKI and CaMKII, but not CaMKIV, were expressed in carotid chemoreceptor cells. Representative examples of the expression pattern of CaMKI are displayed in Figure 1 and of CaMKII in Figures 2 & 3. The successive panels in all figures show nuclear staining (blue), anti-CaMK staining (green), anti-TH staining (red), and an overlay of the latter two (yellow). Each figure shows clusters of chemoreceptor cells, as identified by the

* Correspondence: m_pokorski@hotmail.com
[1]Department of Respiratory Research, Medical Research Center, Polish Academy of Sciences, Warsaw, and Department of Neuropsychology, Institute of Psychology, Opole University, Opole, Poland
[2]Laboratory of Electrophysiology, Clinical Research Center, Murayama Medical Center, MusashiMurayama, Tokyo, Japan
Full list of author information is available at the end of the article

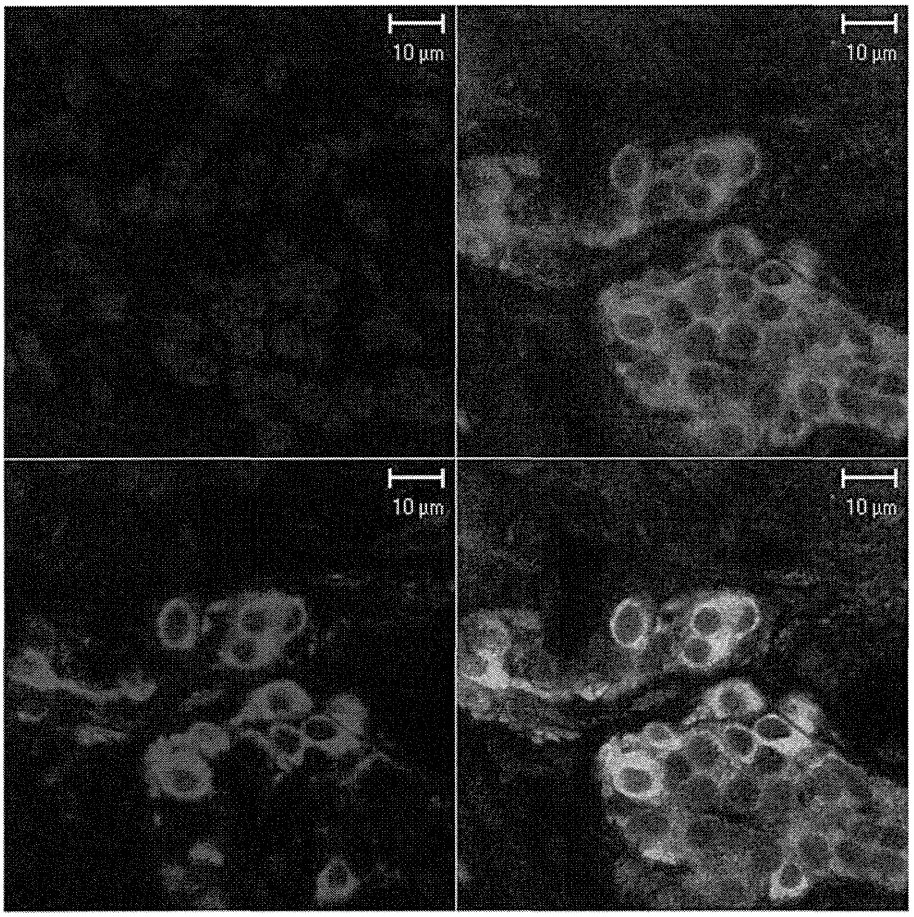

Figure 1 Confocal laser scanning microscopic images of CaMKI immunostaining in the rat carotid body. CaMKI immunostaining in clusters of chemoreceptor cells of the rat carotid body. Consecutive panels show, from left, nuclear staining (blue), anti-CaMKI (green), anti-TH (red), and the overlay of the two fluorescence probes (yellow). CaMKI immunoreactivity overlaps with that of TH in chemoreceptor cells.

TH marker staining, of 10–15 µm in diameter with irregularly oval nuclei. The amount and intensity of both TH and CaMK immunostaining varied between individual cells and clusters of cells, depending on the sectioning of cells. There were differences in the distribution pattern of the two CaMKs, as assessed by visual inspection, based on the density of immunostaining.

The immunostaining of CaMKI had a fine appearance and was distributed throughout the cytoplasm of the chemoreceptor cells, as evidenced by an overlap with the localization of TH expression (Figure 1). There were occasional isles of cells with a degree of mismatch of immunostaining for CaMKI and TH. The mismatch plausibly concerns the cells surrounding a microvessel (Figure 1 - center of the bottom cell cluster), although the method used could not ascertain the exact morphological location. CaMKII, on the other hand, was expressed more intensely in the peripheral layer of the perikaryal cytoplasm, leaving an unstained band encircling the nucleus. The nuclei themselves were devoid of enzyme's expression. The appearance of immunoprecipitates was consistently more granular than that of CaMKI. Double staining for CaMKII and TH showed co-localization of both fluorescent probes. A dovetailed overlap affirms the presence of the protein in the chemoreceptor cells (Figure 2). There were intra-cluster and inter-cluster differences in the intensity of immunostainings (Figure 3). However, the CaMKII immunostaining closely matched that of TH. The expression pattern of CaMKs was highly reproducible in the examined specimens, sampled from carotid bodies of various rats.

CaMKIV could not be conclusively substantiated in chemoreceptor cells. Rather weak and erratic expression of it was seen in the cytoplasm of the cells positive for TH staining and in the nuclei of the cells negative for TH staining. No other fragments of carotid body parenchyma, such as sustentacular cells or nerve endings, were positively identified as expressing any of the CaMKs studied.

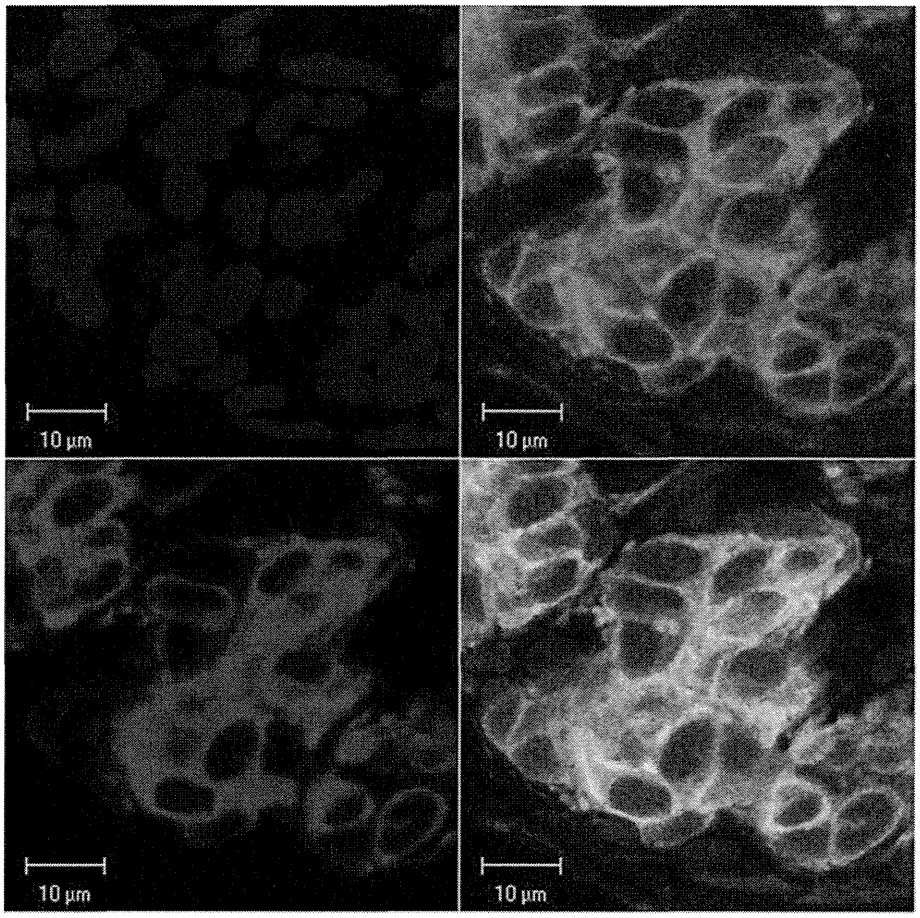

Figure 2 CaMKII immunoprecipitates in the rat carotid body.Localization of CaMKII immunoprecipitates in chemoreceptor cells of the rat carotid body. Consecutive panels show, from left, nuclear staining (blue), anti-CaMKI (green), anti-TH (red), and the overlay of the two fluorescence probes (yellow). CaMKII immunoreactivity overlaps with that of TH in chemoreceptor cells.

Discussion

The present study was designed to identify the presence of individual CaMK proteins in carotid body parenchyma. This purpose stemmed from the premise that for an enzyme to have a possible functional meaning it should be present in the organ in question in the first place. Here we report the presence of CaMKI and CaMKII, but not that of CaMKIV, in the rat chemoreceptor cells. Our study expands on the previous finding of CaMKI expression in the carotid body (Hoshi et al. 2006) in that it is the first visualization of the distribution of individual CaMKs in chemoreceptor cells in the basal, non-stimulated condition.

CaMKII has previously been implicated in hypoxic signaling pathways in PC12 rat pheochromocytoma cells. CaMKII apparently mediates hypoxic activation of *c-fos* gene expression (Premkumar et al. 2000) and it also is influential in inducing the hypoxia-inducible factor-1α (HIF-1α) transcriptional activity through Ca^{2+}-mediated gene regulation in this cell line during intermittent hypoxia (Yuan et al. 2005). By contrast, the CaMKII signaling pathway seems to have no major bearing on the HIF-1α induction in the PC12 cells exposed to sustained hypoxia (Premkumar et al. 2000), which is due to a decreased rate of O_2-dependent proline hydroxylation and, consequently, decreased HIF-1α degradation (Kline et al. 2002).

The PC12 cells share some neurotransmitter composition with the carotid chemoreceptor cells, but that is not necessarily tantamount to their emulating the chemosensing process of the carotid body. The present results give a consistent impression that CaMKII was expressed strongly in chemoreceptor cells. CaMKII encompasses a family of 28 isoforms that are derived from 4 genes and are stratified into α, β, γ, and δ subunits (Hudmon and Schulman 2002). The first two predominate in the brain. It is unclear which subunits predominate in the carotid body and our immunohistochemical study would not discern that. CaMKI is distinct from CaMKII in that its major alpha isoform is localized

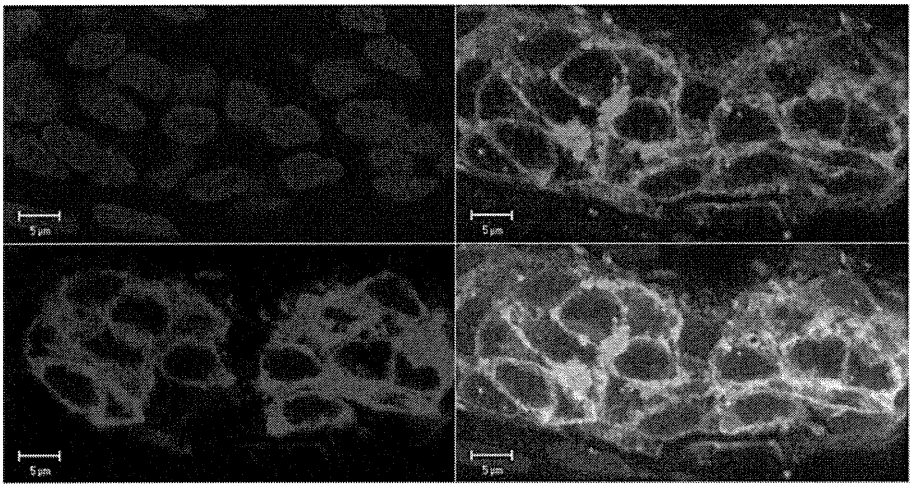

Figure 3 Overlap of CaMKII and TH immunoprecipitates. An example of the overlap of CaMKII and TH immunoprecipitates of varied density in neighboring clusters of chemoreceptor cells in the rat carotid body. Consecutive panels show, from left, nuclear staining (blue), anti-CaMKI (green), anti-TH (red), and the overlay of the two fluorescence probes (yellow).

predominantly to the cytoplasm and is a candidate CaMK for the regulation of gene transcription *in vivo* (Picciotto et al. 1995).

Since both HIF-1α (Lahiri et al. 2007) and hypoxia (Peng et al. 2004) affect O_2-linked adaptable processes in the carotid body and, on the other side, CaMKII is considered a molecular memory enzyme that underlines synaptic plasticity (Fink and Meyer 2002), its potential role in carotid body function raises a research interest. CaMKII is autophosphorylated in a Ca^{2+}/calmodulin-dependent manner, after which it converts to a Ca^{2+}-independent form (Miller and Kennedy 1986). The process prolongs the activity of CaMKII beyond the restoration of a pre-stimulus Ca^{2+} level (Hudmon and Schulman 2002). That, physiologically, translates into the continuation of a stimulus-induced change after the stimulus discontinuation, a phenomenon known in respiratory responses (Pokorski and Serebrovskaya 2009). CaMKII could thus shape the carotid chemoafferent plasticity, the molecular basis of which is not well understood.

The experimental design employed in the current study was but capable of showing the expression of total constitutive CaMKs and did not identify their isoforms which may differ in subcellular distribution and function. Furthermore, the static non-stimulated content of CaMKs is shown, whereas CaMKI regulatory function is usually linked to the stimulus-induced translocation to the postsynaptic densities (Strack and Colbran 1998). Such densities between the abutting chemoreceptor cells or the chemoreceptor cells and sinus nerve endings are the sites of interaction of neurotransmitters, released from secretory vesicles during chemoexcitation, with their specific receptors (Di Giulio et al. 2009). An increase in chemoreceptor cell cytoplasmic Ca^{2+} during instantaneous responses to acute hypoxia (Pokorski et al. 2012) is liable to activate CaMKs. However, it is unknown of how exactly the CaMK signaling coalesces with the hypoxia-sensing cascade in the carotid body.

Conclusions

We herein report the highly reproducible distribution patterns of the CaMKI and CaMKII expressions in carotid chemoreceptor cells. The inference is that CaMK signaling pathways might participate in shaping the chemosensory responses. Confirmation of this biological plausibility requires further studies.

Methods

The study was carried out on tissues dissected from 4 adult, 1 male and 3 female, Wistar rats (weight 140–270 g; age 7–16 wk), handled in accord with the Guiding Principles for Care and Use of Animals of the Physiological Society of Japan. The rats were deeply anesthetized with diethyl ether, and after opening the chest were instantly perfused through the heart with 4% paraformaldehyde in phosphate buffered saline (PBS), pH 7.20. The carotid bodies were dissected bilaterally from the carotid bifurcation area. The nearby sympathetic superior cervical ganglions also were dissected to be used as reference specimens for both CaMKs and tyrosine hydroxylase (TH), a marker of chemoreceptor cells. Additionally, the brain was extracted from the skull and the hippocampus was cut out for positive CaMKs controls. All the tissues were immersed in the same fixative in which they were postfixed for 1.5 h and then cryoprotected in 30% sucrose at 4°C until further use.

Sections of the carotid body (10 μm thick), superior cervical ganglion (15 μm thick), and hippocampal

(30 μm thick) tissues were made (CM1900 cryostat, Leica Instruments, Nussloch, Germany) and attached to glass slides coated with poly-L-lysine. Sections from all the tissues were processed on the same glass slide for a given CaMK.

The immunohistochemical procedures were performed in room temperature and consisted of five successive steps. I – solubilization of specimens in 0.3% Triton X-100 in PBS for 15 min; II – blocking the nonspecific binding with 5% normal goat serum for 30 min; III – overnight incubation with primary rabbit IgG rabbit antibodies against CaMKI, CaMKII, and CaMKIV (dilution 1:1000, 1:1000, and 1 3 μg/ml, respectively) and with a PCTH-7 mouse monoclonal IgG antibody against TH for double staining to confirm the chemoreceptor cell localization of immunostaining; IV – 1 h incubation with secondary goat Alexa Fluor 488-conjugated antirabbit + goat Alexa Fluor 594-conjugated antimouse antibodies diluted at 1:2000 (Alexa Flour; Molecular Probes, Eugene, OR) in the environment protected from light; and V – nuclear staining with 4',6-diamidino-2-phenylindole (DAPI; Sigma-Aldrich, St. Louis, MO). Steps III, IV, and V were followed by several sequential washes of specimens in PBS. Finally, the specimens were covered with an embedding medium and examined by visual inspection and photographed under a confocal laser scanning microscope and workstation (LSM 5 Pascal; Carl Zeiss, Jena, Germany).

Antibodies against CaMKI were produced in-house. Briefly, the entire coding region of rat CaMKIα was amplified by PCR and inserted in frame to pGEX4T-1 expression vector (Amersham Biosciences, Piscataway, NJ). The glutathione S-transferase (GST)-CaMKIα fusion protein was induced in *E. coli* in the presence of isopropyl-1-thio-β-D-galactoside. The fusion protein was then purified from a soluble extract by glutathione-Sepharose 4B (Amersham Biosciences, Piscataway, NJ) according to the manufacturer's protocol. Two female New Zealand rabbits were immunized by repeated intradermal injections of the fusion protein emulsified with an equal volume of Freund's adjuvant. The antibody against CaMKI was purified by a protein A-sepharose 4B column, followed by the A-sepharose 4B column coupled with GST-CaMKIα. Western blots showed that the antibody reacted with CaMKIα and δ, but not β2 and γ1 in a single band. Antibodies against CaMKIV were made according to the method described previously (Sakagami et al. 1994) and those against CaMKII were generously provided by Prof. Kohji Fukunaga of Tohoku University Graduate School of Pharmaceutical Sciences.

Positive controls showed the CaMKs immunostainings in the hippocampus, which was particularly relevant regarding the CaMKIV that appeared as streaks of stained neuronal nuclei. The CaMKs and TH closely overlapped in the sympathetic neurons of the superior cervical ganglion, as is reported in the literature (Arciszewski et al. 2004). Negative controls, in which the primary antibody was omitted, failed to express immunostaining. Thus, both positive and negative controls (not shown) verified the soundness of the immunostaining.

Competing interests

The authors declare they have no competing interests in relation to this article.

Authors' contributions

All authors participated in the preparation of the manuscript, and read and approved the final manuscript.

Acknowledgements

MP was supported by a JSPS fellowship. YO was supported by Grants-in-Aid for Science Research from the Ministry of Education, Culture, Sports, Science and Technology of Japan and by Health and Labor Sciences Research Grants of Japan.

Author details

[1]Department of Respiratory Research, Medical Research Center, Polish Academy of Sciences, Warsaw, and Department of Neuropsychology, Institute of Psychology, Opole University, Opole, Poland. [2]Laboratory of Electrophysiology, Clinical Research Center, Murayama Medical Center, MusashiMurayama, Tokyo, Japan. [3]Department of Anatomy, Kitasato University School of Medicine, Sagamihara, Kanagawa, Japan.

Received: 23 July 2012 Accepted: 22 August 2012
Published: 27 August 2012

References

Arciszewski MB, Zacharko A, Lalak R (2004) Co-expression of tyrosine hydroxylase, dopamine beta-hydroxylase and neuropeptide Y in the sympathetic neurons projecting to the submandibular gland in the sheep. Anat Embryol (Berl) 208:161–167

Di Giulio C, Angelucci S, Di Ilio C, Eleuterio E, Di Giuseppe F, Sulpizio M, Verratti V, Pecyna M, Pokorski M (2012) Proteomic analysis of the carotid body: a preliminary study. Adv Exp Med Biol 756:349–353. doi:10.1007/978-94-007-4549-0_42

Di Giulio C, Antosiewicz J, Walski M, Petruccelli G, Verratti V, Bianchi G, Pokorski M (2009) Physiological carotid body denervation during aging. Adv Exp Med Biol 48:257–63

Fink CC, Meyer T (2002) Molecular mechanisms of CaMKII activation in neuronal plasticity. Curr Opin Neurobiol 12:293–299

Hook SS, Means AR (2001) Ca^{2+}/CaM-dependent kinases: from activation to function. Annu Rev Pharmacol Toxicol 41:471–505

Hoshi H, Sakagami H, Owada Y, Kondo H (2006) Localization of Ca/calmodulin-dependent protein kinase I in the carotid body chief cells and the ganglionic small intensely fluorescent (SIF) cells of adult rats. Adv Exp Med Biol 580:87–92

Hudmon A, Schulman H (2002) Structure-function of the multifunctional Ca^{2+}/calmodulin-dependent protein kinase II. Biochem J 364:593–611

Kline DD, Peng YJ, Manalo DJ, Semenza GL, Prabhakar NR (2002) Defective carotid body function and impaired ventilatory responses to chronic hypoxia in mice partially deficient for hypoxia-inducible factor 1 alpha. Proc Natl Acad Sci USA 99:821–826

Lahiri S, Antosiewicz J, Pokorski M (2007) A common oxygen sensor regulates the sensory discharge and glomus cell HIF-1α in the rat carotid body. J Physiol Pharmacol 58(Suppl 5):327–333

Miller SG, Kennedy MB (1986) Regulation of brain type II Ca^{2+}/calmodulin-dependent protein kinase by autophosphorylation: A Ca^{2+}-triggered molecular switch. Cell 44:861–870

Obeso A, Rocher A, Fidone S, Gonzáles C (1992) The role of dihydropyridine-sensitive Ca^{2+} channels in stimulus-evoked catecholamine release from chemoreceptor cells of the carotid body. Neuroscience 47:463–472

Peng Y-J, Rennison J, Prabhakar NR (2004) Intermittent hypoxia augments carotid body and ventilatory response to hypoxia in neonatal rat pups. J Appl Physiol 97:2020–2025

Picciotto MR, Zoli M, Bertuzzi G, Nairn AC (1995) Immunochemical localization of calcium/calmodulin-dependent protein kinas I. Synapse 20:75–84

Pokorski M, Faff L, Di Giulio C (2012) Hypoxic redistribution of iron and calcium in the cat glomus cells. Adv Exp Med Biol 758. doi:10.1007/978-94-007-4584-1_13

Pokorski M, Serebrovskaya T (2009) Intermittent hypercapnia. In: Xi L, Serebrovskaya TV (eds) Intermittent hypoxia: from molecular mechanisms to clinical applications. Nova, Hauppauge, New York, pp 261–274, Chapter 12

Premkumar DR, Mishra RR, Overholt JL, Simonson MS, Cherniack NS, Prabhakar NR (2000) L-type Ca^{2+} channel activation regulates induction of c-fos transcription by hypoxia. J Appl Physiol 88:1898–1906

Sakagami H, Tsubochi H, Kondo H (1994) Immunohistochemical localization of Ca^{2+}/calmodulin-dependent protein kinase type IV in the peripheral ganglia and paraganglia of developing and mature rats. Brain Res 666:173–181

Strack S, Colbran RJ (1998) Autophosphorylation-dependent targeting of calcium/calmodulin-dependent protein kinase II b the NR2B subunit of the N-methyl-D-aspartate receptor. J Biol Chem 273:20689–20692

Yuan G, Nanduri J, Bhasker CR, Semenza GL, Prabhakar NR (2005) Ca^{2+}/calmodulin kinase-dependent activation of hypoxia inducible factor 1 transcriptional activity in cells subjected to intermittent hypoxia. J Biol Chem 280:4321–4328

Zara S, Pokorski M, Cataldi A, Porzionato A, De Caro R, Antosiewicz J, Di Giulio C (2012) Development and aging are oxygen-dependent and are correlated with VEGF and NOS along life span. Adv Exp Med Biol :223–228. doi:10.1007/978-94-007-4549-0_28

doi:10.1186/2193-1801-1-16
Cite this article as: Pokorski *et al.*: **Calcium/calmodulin-dependent protein kinases in the carotid body: an immunohistochemical study.** *SpringerPlus* 2012 **1**:16.

Chapter 9
Time-Course of Ventilation, Arterial and Pulmonary CO_2 Tension During CO_2 Increase in Humans

Toru Satoh, Yasumasa Okada, Yasushi Hara, Fumio Sakamaki, Shingo Kyotani, Takeshi Tomita, Noritoshi Nagaya, and Norifumi Nakanishi

Abstract A change of ventilation (VE), $PaCO_2$ (arterial CO_2 tension) and $PvCO_2$ (pulmonary arterial CO_2 tension) with time was not evaluated precisely during exercise or CO_2 rebreathing in humans. In this study, changes of these variables with time were fitted to exponential curves {y=Exp (x/ T+A)+k} and compared. When exercise pulmonary hemodynamics was examined in 15 cardiac patients to decide therapies, we asked the patients to undergo CO_2 rebreathing using air with supplementation of consumed O_2. Arterial and pulmonary blood was drawn every minute. During exercise, T was 28.2±8.4 and 26.8±12.4, and A was 0.80±0.50 and 0.50±0.90 in VE and $PvCO_2$, respectively, with no statistical differences. During CO_2 rebreathing, T was 18.6±5.8, 41.8±38.0 and 21.6±9.7 and A was 0.39±0.67, 1.64±1.35 and 0.17±0.83 in VE, $PaCO_2$ and $PvCO_2$, respectively, with statistical difference of $PaCO_2$ from other variables, suggesting that VE and $PvCO_2$ showed same mode of change according to time but $PaCO_2$ did not.

Keywords Ventilation • $PaCO_2$ • $PvCO_2$ • CO_2 rebreathing

9.1 Introduction

A change of VE, $PaCO_2$ and $PvCO_2$ with time was not evaluated precisely during CO_2 increasing state like exercise or CO_2 rebreathing in humans. Gelfand and Lambertsen (1973) studied time course of ventilatory change by abruptly adding and removing CO_2 in inhaled air and reported that there were three respiratory components with differing onset lag time and time constant. We did a similar analysis of $PaCO_2$ and $PvCO_2$ as well as VE during CO_2 rebreathing and exercise tests in 15 cardiac patients. We performed exercise test with arterial and pulmonary arterial blood sampling to make therapeutic

T. Satoh (✉)
Cardiology Division, Department of Medicine, Kyorin University School of Medicine,
Shinkawa 6-20-2, Mitakashi, Tokyo 181-8611, Japan
tsatoh2008@me.com

Y. Okada
Department of Medicine, Keio University Tsukigase Rehabilitation Center,
Amagiyugashima-cho 410-3293, Japan

Y. Hara • F. Sakamaki • S. Kyotani • T. Tomita • N. Nagaya • N. Nakanishi
Division of Cardiology and Pulmonary Circulation, Department of Medicine,
National Cardiovascular Center, Suita, Osaka, 565-8565, Japan

C.A. Nurse et al. (eds.), *Arterial Chemoreception: From Molecules to Systems*,
Advances in Experimental Medicine and Biology 758, DOI 10.1007/978-94-007-4584-1_9,

decisions for cardiac patients. Then we asked them to undergo CO_2 rebreathing test after explanation of the study purpose to elucidate CO_2 and ventilatory kinetics and know ventilatory control mechanics. We fitted the plotting of $PaCO_2$, $PvCO_2$ and VE with time, to exponential curve. Time constant and fixed constant values of the resultant equations in each variable were calculated and compared each other to see the relation of $PaCO_2$, $PvCO_2$ and ventilation.

The results suggest that the fitted equation of VE with time was statistically different from the fitted equation of $PaCO_2$ with time, but not from the fitted equation of $PvCO_2$ with time. Implication of our results is that VE and $PvCO_2$ are changed identically, but it must await further study that this relation is a cause or a result. We report this result because it may add new insights to ventilation research in terms of CO_2 kinetics.

9.2 Methods

9.2.1 Study subjects

The study subjects were 15 patients with cardiac disease, who underwent pulmonary hemodynamic investigations in order to help determine their treatment plans. Eleven had mitral valvular heart disease (4 dominant mitral stenosis, 4 dominant mitral regurgitation and 3 combined mitral stenosis and regurgitation), 2 had dilated cardiomyopathy, and 2 had chronic pulmonary thromboembolism. No patient had ventilatory disorder. Their age was 51 ± 15 years (mean $\pm$ S.D.). Eight patients were male and seven were female. The purpose, protocol and risks of the present study were fully explained, and written informed consent was obtained from each patient.

9.2.2 Protocol

The patients performed exercise on an upright cycle ergometer 4 h after their usual breakfast and medication, with a Swan-Ganz catheter inserted via the right internal jugular vein into the pulmonary artery and a fine arterial catheter inserted via the left radial artery. They pedaled at a speed of 55 rpm without any added load for 1 min. Then the load was increased by 1 W/ 4 s (15 W/ min) to the symptom-limited maximum. Continuous hemodynamic monitoring, including that of arterial and pulmonary arterial pressures, and expired gas analysis (AE280, Minato Medical Instruments, Osaka) were performed every 6 s throughout the period of exercise. Expired ventilation (VE) was measured by hot-wire flowmeter. Arterial and pulmonary arterial blood samples were collected before exercise and every minute during exercise for blood gas analysis. On the same day, 3 h after lunch, the subjects were tested during CO_2 rebreathing using a bag containing 6 l of air, with the same hemodynamic, expired gas and blood gas analyses as during exercise. Oxygen consumption (VO_2) was determined in advance and an equal amount of O_2 was supplemented into the rebreathing bag to maintain a constant inspired O_2 concentration throughout the rebreathing test.

9.2.3 Fitting to Exponential Curve

VE, $PaCO_2$ and $PvCO_2$ were plotted against time. As the relations resembled exponential curve, they were fitted to $y = \mathrm{Exp}(x / T + A) + k$. Figure 9.1 demonstrated a representative case during CO_2 rebreathing.